

PERFORMANCE OF ANL ECR BREEDER WITH LOW MASS BEAMS

R. Vondrasek, S. Kutsaev, R. Pardo, R. Scott, Argonne National Laboratory, Argonne, IL 60439, U.S.A.

P. Delahaye, and L. Maunoury, Grand Accélérateur National d'Ions Lourds (GANIL), CEA/DSM-CNRS/IN2P3, Blvd Henri Becquerel, 14076 Caen, France

Abstract

The Californium Rare Isotope Breeder Upgrade (CARIBU) is a new radioactive beam facility for the Argonne Tandem Linac Accelerator System (ATLAS). The facility utilizes a ^{252}Cf fission source coupled with an electron cyclotron resonance (ECR) ion source to provide radioactive beam species for the ATLAS experimental program. The californium fission fragment distribution provides nuclei in the mid-mass range which are difficult to extract from production targets using the isotope separation on line (ISOL) technique and are not well populated by low-energy fission of uranium. To date the charge breeding program has focused on optimizing these mid-mass beams, achieving high charge breeding efficiencies of both gaseous and solid species including 14.7% for the radioactive species $^{143}\text{Ba}^{27+}$. In an effort to better understand the charge breeding mechanism, we have recently focused on the low-mass species sodium and potassium which up to present have been difficult to charge breed efficiently. Unprecedented charge breeding efficiencies of 10.1% for $^{23}\text{Na}^{7+}$ and 17.9% for $^{39}\text{K}^{10+}$ were obtained injecting stable Na^+ and K^+ beams from a surface ionization source.

INTRODUCTION

The development of ECR charge breeders is being pursued by many groups [1-8] with a particular concern being the efficient charge breeding of light ion species which up to present has been problematic [9,10]. The GANIL ion source group is pursuing a new 1+ to n+ charge breeding system for the SPIRAL project utilizing an ECR ion source with the efficient charge breeding of light nuclei being of high importance. Previously confined to gaseous elements, new versatile 1+ sources will be used to extend the range of elements available for post-acceleration to condensable elements. During on-line tests with such ion sources, radioactive isotopes of 9 new elements have already been ionized: isotopes of the alkali (Li, Na, K, Rb) metallic (Al, Fe, Cu, Mn) and halogen (Cl) elements were all produced from the FEBIAD ion source except for the alkali ion Li which was only surface ionized. While the new 1+ sources allow for the production of a wider range of elements, achieving a high charge breeding efficiency in the ECR remains a critical step. With this in mind, a new ECR charge breeder is being designed for the SPIRAL upgrade. The future ECR charge breeder will be based on an upgrade of an existing Phoenix ECR ion source which was formerly tested at ISOLDE, CERN [11,12]. The upgraded charge breeder will include a number of modifications inspired from the Argonne National Laboratory (ANL) ECR charge

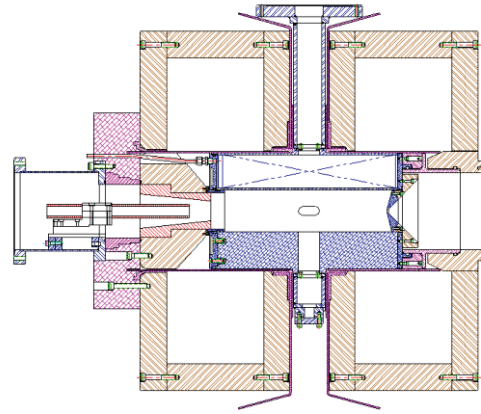


Figure 1: Schematic of the ANL ECR charge breeder. The 1+ beam is injected from the left through the grounded stainless steel tube. The tapered iron plug is highlighted with diagonal red hatching. The radial slots where the RF is launched are visible on the source mid-plane.

breeder: the injection of two RF frequencies (one fixed 14 GHz and one variable 8-18 GHz); complete cylindrical symmetry at the injection side; on-line adjustment of the grounded tube position; and a vacuum level around a few 10^{-8} mbar.

THE ANL ECR CHARGE BREEDER

In its final configuration, the CARIBU facility [13] will use a 1 Ci ^{252}Cf source to produce fission fragments which will be thermalized and collected by a helium gas catcher into a particle beam with a charge of 1+ or 2+. An ECR ion source functions as a charge breeder (ECRCB) [14,15] in order to raise the ion charge sufficiently for acceleration in the ATLAS linac.

The charge breeder is a room temperature ECR operating at 10-14 GHz with an open-structure NdFeB hexapole (see scheme in Fig. 1). The six radial ports which are each 17 x 41 mm in size act as pumping channels resulting in a plasma chamber pressure of 5×10^{-8} Torr. They also serve to introduce the RF and support gas into the plasma chamber. This eliminates the need for cut-outs in the injection side iron plug and results in a large peak and highly symmetric axial magnetic field where the ions enter the plasma. This scheme differs from other ECR charge breeders in existence which are closed hexapole devices with axial RF injection. For the ANL ECRCB, the low charge-state ions are introduced into the plasma through a grounded stainless steel tube mounted on a linear motion stage. The stage has a 30 mm range of

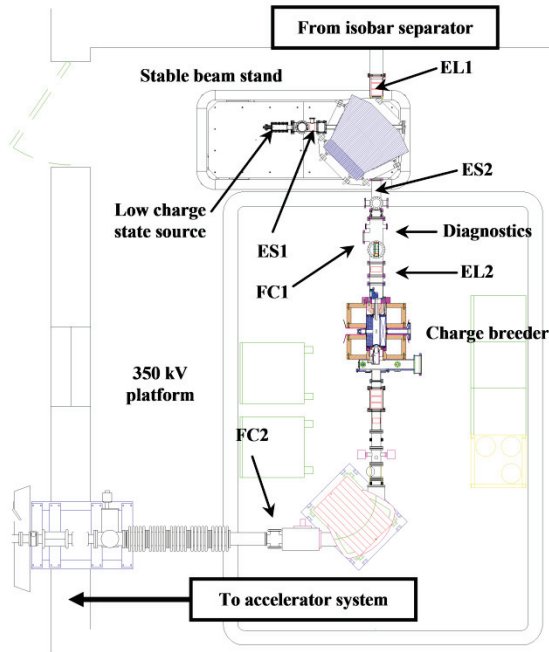


Figure 2: Floor plan of the charge breeder system showing the stable beam stand, the electrostatic steerers (ES1 & ES2), the einzel lenses (EL1 & EL2), the faraday cups (FC1 & FC2), the diagnostics location, and the ECRCB.

travel, and thus the deceleration point of the low-charge state ions can be adjusted on-line without disturbing the source conditions. The ECRCB is designed to operate at a 50 kV potential although for these tests the voltage was maintained at 30 kV.

CHARGE BREEDING RESULTS

Stable 1+ beams of sodium and potassium were produced by a surface ionization source with injected intensities ranging from 500 enA to as low as 2 enA. The transport system, shown in Fig. 2, consists of two electrostatic steerers, an einzel lens, a set of 4-jaw slits directly after the surface ionization source for controlling beam intensity, and a double set of 4-jaw slits at the image point of the 90 degree analyzing magnet spaced 16.5 cm apart. The slits serve to control the beam emittance and define the beam trajectory going into the ECRCB easing the transition between stable and radioactive beam breeding. The diagnostics region includes a fully shielded Faraday cup for measuring the 1+ beam (FC1) and a silicon surface barrier detector (SBD) for measuring radioactive beams via beta decay. After the 1+ beam has been injected into the charge breeder through the grounded tube, a ΔV voltage between the 1+ source and the ECRCB decelerates the ions into the plasma region where a sub-set of them are ionized and captured by the plasma [16].

Table 1: Summary of Charge Breeding Results for Mid-Mass Species

Ion	Charge state	Efficiency (%)	A/Q
⁸⁴ Kr	17+	15.6	4.94
⁸⁵ Rb	19+	13.7	4.47
¹²⁹ Xe	25+	13.4	5.16
¹³³ Cs	27+	13.0	4.93
¹⁴³ Cs(1+) (<i>t</i> _{1/2} =1.79 s)	27+	11.7	5.30
¹⁴³ Ba (2+) (<i>t</i> _{1/2} =14.3 s)	27+	14.7	5.30

After charge breeding, the intensity of the mass analyzed n+ ions is observed on either a Faraday cup (FC2) for the stable beams or a SBD at this same location for the radioactive beams. The breeding efficiency and time are determined by pulsing the incoming 1+ beam, using the electrostatic steerer (ES1) voltage, and measuring the n+ response on FC2. A summary of achieved charge breeding efficiencies for the mid-mass species is given in Table 1.

The first charge breeding test was with Rb-85 in order to establish a performance benchmark. While the best efficiency for ⁸⁵Rb²⁰⁺ was 11.4% (lower than the record of 13.2%), the higher charge states performed well and surpassed the previous achieved efficiencies by a factor of 2 for 23+ through 25+ (shown in Fig. 3).

The first test of light element breeding was performed with a sodium pellet loaded into the surface ionization source. The system was checked for leaks and achieved a base pressure of 2.5 x 10⁻⁸ Torr without plasma. With the ECRCB running a base plasma of helium, the pressure increased to 6.6 x 10⁻⁸ Torr. A beam of Na⁺ with an intensity of 12.6 nA was injected into the ECRCB resulting in a ²³Na⁸⁺ breeding efficiency of 6.0%. The addition of oxygen to the plasma reduced the breeding efficiency to 5.0%.

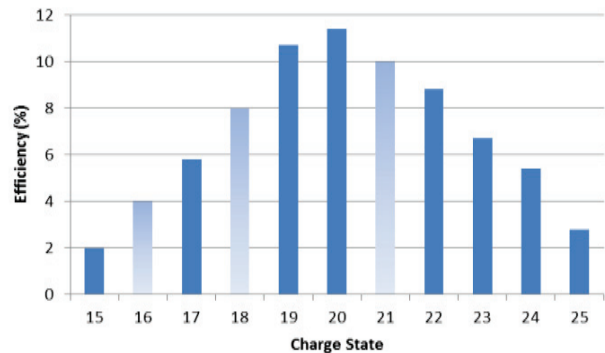


Figure 3: Efficiency of Rb-85 as a function of charge state. Charge states 16+, 18+, and 21+ were obscured by intense background peaks and their values have been extrapolated.

A second test of the sodium breeding efficiency took place where the base plasma of He-4 was replaced with He-3. With a pure He-4 plasma, the source was producing $^{23}\text{Na}^{8+}$ with an efficiency of 7.6%. As only the gas mixture was altered such that the plasma was entirely He-3, the efficiency for $^{23}\text{Na}^{8+}$ remained at 7.6%. Further optimization of the injection optics, solenoid coils, gas pressure, and ΔV ultimately produced $^{23}\text{Na}^{8+}$ with a 8.1% efficiency and $^{23}\text{Na}^{7+}$ with a 9.0% efficiency. Further optimization on $^{23}\text{Na}^{7+}$ resulted in a breeding efficiency of 10.1%. Changing the base plasma back to He-4 produced no change in efficiency.

A potassium pellet was then installed in the surface ionization source. The ECRCB was restarted and immediately achieved a 4.2% breeding efficiency for $^{39}\text{K}^{10+}$ with 14.8 nA of K^+ injected into the source. As stated earlier, the 4-jaws after the surface ionization source are used to control the 1+ beam intensity and emittance. These slits also play a role in defining the beam trajectory. By adjusting these slits while observing the charge bred beam intensity, an optimum setting was found which produced a 13.8% breeding efficiency for $^{39}\text{K}^{10+}$ with 16.5 nA injected into the ECRCB. Further optimization of the optics elements, the support gas, and grounded tube position resulted in a maximum breeding efficiency of 17.9 % for $^{39}\text{K}^{10+}$. This represents the highest charge breeding efficiency to date for an ECR ion source. It is possible to achieve such high efficiencies due to the charge state distribution for the lower masses narrowing and resulting in an increase of the single charge state population. A complete list of the light element charge breeding efficiencies is shown in Table 2. The higher ^{39}K charge states were obscured by other stable beams and could not be reliably identified. As with sodium, it was observed that adding oxygen to the mixing gas was not beneficial. The breeding time for $^{39}\text{K}^{10+}$ was determined to be 160 msec from injection of the 1+ beam to full intensity of the 10+ beam and 150 msec for the $^{39}\text{K}^{9+}$ case.

Table 2: Summary of Charge Breeding Results for Sodium and Potassium

Ion	Charge state	Efficiency (%)	A/Q
^{23}Na	6+	6.6	3.83
	7+	10.1	3.29
	8+	8.6	2.87
	9+	3.4	2.56
^{39}K	7+	3.0	5.57
	8+	4.9	4.87
	9+	15.6	4.33
	10+	17.9	3.90

BEAM INJECTION SIMULATIONS

The work with the ANL ECRCB has shown that the large performance disparity between gaseous and nongaseous elements has been greatly diminished. For identical source conditions, the only difference between the two cases is the wall sticking coefficient. In the case of gaseous elements, many of the ions which hit the plasma chamber surfaces are quickly re-emitted into the plasma. In contrast, the solid elements condense onto the plasma chamber surfaces meaning that any incoming particles that do impact a surface are lost to the plasma. It can be surmised that the present injection optics and source conditions reduce the number of incoming ions lost to the plasma chamber surfaces before capture into the plasma.

One of the possible contributing factors to the high breeding efficiencies is the iron plug design. The lack of cut-outs in the iron plug results in a large peak magnetic field which is symmetric where the ions enter the plasma chamber. 3D magnetic field calculations of the ANL ECRCB using Computer Simulation Technology Electromagnetic Studio [17] were performed taking into account the coils, iron, and hexapole. The coil currents were set to the values used for charge breeding resulting in a peak axial field of 1.2 T. The hexapole wall field was measured to be 0.84 T. Two cases were evaluated – one for radial RF injection and one for axial RF injection which included cut-outs in the iron plug. The results were then plotted as horizontal planes passing through the charge breeder with the central axis of the source at the 0,0 coordinate. The view shown in Fig. 4 is the horizontal plane directly in front of the face of the iron plug. The simulations showed that the magnetic field for the case with the cut-outs was asymmetric with the magnetic field center offset from the ion source geometric center.

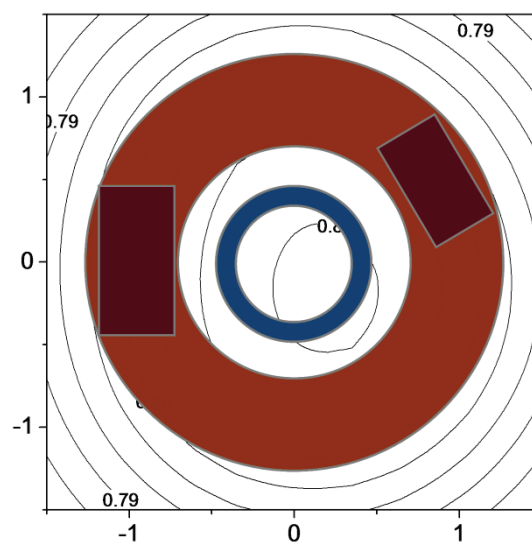


Figure 4: The magnetic field in the injection region with the waveguide cut-outs. The overlaid shapes show the position of the transfer tube in blue, the iron plug in brown, and the waveguides in red.

While the simulations showed that the magnetic field was asymmetric, the effect on the incoming low charge state ions was not well established. Further simulations were performed with test particles of $^{133}\text{Cs}^+$ ions injected into the ECRCB using the full 3D magnetic and electric field configuration. The simulations assumed: injection of $^{133}\text{Cs}^+$ ions with an energy spread of 1 eV and emittance of 3π mm mrad (the measured values of the beam coming from the CARIBU gas catcher), the running condition coil currents, and 30 kV injection with a ΔV of -20 V. Fig. 5 shows that in the case of the symmetric injection field, the 1+ ions penetrate deep into the plasma chamber almost reaching the extraction aperture. For the asymmetric case, the ions do not travel far into the plasma and hence capture into the plasma is diminished. The simulations were only intended to model the trajectories of the incoming 1+ ions and do not take into account any ion/plasma interactions.

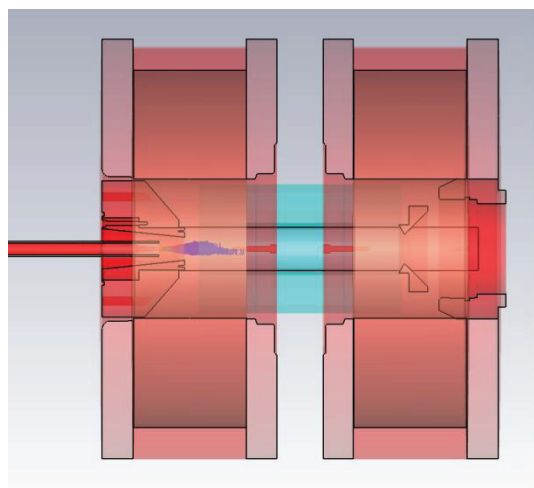
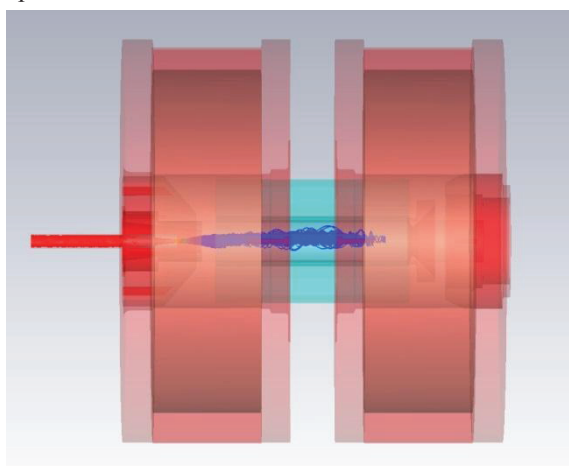


Figure 5: Simulation of $^{133}\text{Cs}^+$ injected into the ECRCB at 30 kV with ΔV of -20 V. The top figure is the case with radial RF injection and no cut-outs in the iron plug. The bottom figure assumes identical conditions except that the RF is now injected axial and the iron plug has cut-outs to accommodate the waveguides.

SUMMARY AND OUTLOOK

With the charge breeding efficiencies of ^{23}Na and ^{39}K meeting or surpassing that of the heavier elements, the previously observed trend of decreased performance for the light elements [18] is after a careful and complete parameter optimization not seen in this work. In [9], it was proposed that the incoming ions are slowed by elastic ion-ion collisions with the plasma ions. The optimum slowing down occurs when the incoming ions enter into the plasma with a velocity roughly equal to the average velocity of the plasma ions. A velocity mismatch will result in a weaker slowing down force and hence a lower breeding efficiency. Additionally, good beam optics are required for the efficient capture of the very low velocity incoming ions.

In the case of sodium, assuming an oxygen plasma with an ion temperature of 2 eV, the sodium ion energy required to match the ion velocities and attain the optimum slowing coefficient is 2.9 eV. In source tests with an oxygen plasma, the realized charge breeding efficiency of $^{23}\text{Na}^{8+}$ was 5.0%. It was only with a helium plasma that the quoted efficiency of 8.6% was achieved. In this case, the sodium ions would have an energy of 11.5 eV for optimum slowing, very similar to the rubidium case and requiring less stringent requirements on the beam optics due to the increased velocity.

Compared to the couple of percent obtained thus far with other charge breeders, the charge breeding efficiencies for light condensable ions have been dramatically enhanced during the course of these experiments, approaching efficiencies usually observed for noble gases. This tends to indicate that the relevant parameters – beam emittance and trajectory, gas mixing, magnetic field alignment and homogeneity - have been optimized. Further investigation will be performed at ANL with an emittance meter installed in the 1+ beam line. In light of these latest results, special care will be taken in the SPIRAL upgrade for the optimization and control of the 1+ ion source beam optics and emittance.

ACKNOWLEDGEMENTS

This work was supported by the U.S. Department of Energy, Office of Nuclear Physics, under contract number DE-AC02-06CH11357. The SPIRAL upgrade activities are supported by the European Union's Seventh Framework Programme under grant agreement n°262010 within the ENSAR project, and within ERA-NET NuPNET as part of the EMILIE project.

REFERENCES

- [1] R. Vondrasek, A. Levand, R. Pardo, G. Savard, and R. Scott, *Rev. Sci. Instrum.* 83, 02A913 (2012).
- [2] S.C. Jeong, M. Oyaizu, N. Imai, Y. Hirayama, H. Ishiyama, H. Miyatake, K. Niki, M. Okada, Y.X. Watanabe, Y. Otokawa, A. Osa, and S. Ichikawa, *Rev. Sci. Instrum.* 83, 02A910 (2012)
- [3] T. Lamy, J. Angot, P. Sortais, T. Thuillier, and A. Galatà, *Rev. Sci. Instrum.* 83, 02A909 (2012)

- [4] Prospects for advanced electron cyclotron resonance and electron beam ion source charge breeding methods for EURISOL
- [5] P. Delahaye, A. Galata, J. Angot, G. Ban, L. Celona, J. Choinski, P. Gmaj, A. Jakubowski, P. Jardin, T. Kalvas, et al, *Rev. Sci. Instrum.* 83, 02A906 (2012)
- [6] G. Tabacaru, D. P. May, J. Arje, G. Chubarian, H. Clark, G. J. Kim, and R. E. Tribble, *Rev. Sci. Instrum.* 83, 02A905 (2012)
- [7] F. Ames, R. Baartman, P. Bricault, K. Jayamanna, T. Lamy, and M. McDonald, *Rev. Sci. Instrum.* 81, 02A903 (2010)
- [8] Damayanti Naika, Vaishali Naika, Alok Chakrabartia, S. Dechoudhurya, Sumanta Kumar Nayaka, H.K. Pandeya, Takahide Nakagawab, *Nucl. Instrum. and Meth. A* 547, 270 (2005)
- [9] R. Geller, T. Lamy and P. Sortais, *Rev. of Scient. Instrum.* 77 (2006) 03B107
- [10] F. Wenander, *NIM B*, 266 (2008) 4346-4353
- [11] M. Marie-Jeanne, PhD thesis, Université Joseph Fourier (2009)
- [12] P. Delahaye, C. J. Barton, K. Connell, T. Fritioff, O. Kester, T. Lamy, M. Lindroos, P. Sortais, G. Tranströmer, and F. Wenander, *Rev. Sci. Instrum.* 77, 03B105 (2006)
- [13] R. Pardo, G. Savard, S. Baker, C. Davids, E. F. Moore, R. Vondrasek, G. Zinkann, *NIM-B* 261, Issues 1-2 (2007) 965
- [14] R. C. Vondrasek, R. Scott, J. Carr, R. C. Pardo, *Rev. Sci. Instrum.* 79, 02A901 (2008)
- [15] R. Vondrasek, A. Kolomiets, A. Levand, R. Pardo, G. Savard, R. Scott, *Rev. Sci. Instrum.* 82, 053301 (2011)
- [16] R. Geller, *Rev. Sci. Instrum.* 71, (2000) 612
- [17] Computer Simulation Technology Electromagnetic Studio, www.cst.com
- [18] P. Delahaye, O. Kester, C. Barton, T. Lamy, M. Marie-Jeanne, F. Wenander, *Eur. Phys. J. A* 46, 421–433 (2010)